Nano Energy 55 (2019) 534–540

Contents lists available at ScienceDirect

Nano Energy

journal homepage: www.elsevier.com/locate/nanoen

Full paper

Standard and figure-of-merit for quantifying the performance of pyroelectric nanogenerators

Kewei Zhang[a], Yuanhao Wang[b,*], Zhong Lin Wang[a,c,d,e,**], Ya Yang[a,c,d,**]

[a] CAS Center for Excellence in Nanoscience, Beijing Institute of Nanoenergy and Nanosystems, Chinese Academy of Sciences, Beijing 100083, PR China
[b] Xinjiang Technical Institute of Physics & Chemistry, Chinese Academy of Science, Urumqi, Xinjiang 830011, PR China
[c] School of Nanoscience and Technology, University of Chinese Academy of Sciences, Beijing 100049, PR China
[d] Center on Nanoenergy Research, School of Physical Science and Technology, Guangxi University, Nanning 530004, PR China
[e] School of Material Science and Engineering, Georgia Institute of Technology, Atlanta, GA 30332-0245, USA

ARTICLE INFO

Keywords:
Pyroelectric nanogenerators
Figure-of-merits
Heat energy
Charge-voltage cycle

ABSTRACT

Pyroelectric nanogenerators have emerged as an effective approach for the energy of the new-era, the era of internet of things, with a great potential for harvesting waste heat energy. Here, we present the figure-of-merit for quantifying the output of a pyroelectric nanogenertor. The charge-voltage cycle during temperature cycling has been experimentally performed on a PVDF film and PZT ceramic material. Output energy of 2.53 μJ per cycle and 2.59 mJ per cycle is presented at temperature cycling of 23 K (from 300 to 323 K) and 8 K (from 300 to 308 K) for the PVDF and PZT, respectively. The practicability of the derived figure-of-merit as a universal standard for pyroelectric nanogenerator is further experimentally confirmed and compared with previous results. We believe that it could be useful for optimizing the performance of pyroelectric nanogenerators from both material and structural aspects as well as estimating the generated electricity based on maximum temperature cycling.

1. Introduction

With the growing crisis of energy shortage and environment pollution, great efforts are being devoted to abounding new-era energies. [1–3] Meanwhile, a large amount of heat energy is wasted in our surrounding environment, including human body, vehicle exhaust, and temperature changes caused by convection and solar radiation. [4–8] Taking advantage of pyroelectric effect, a pyroelectric nanogenerator can convert this waste heat energy (time-dependent temperature fluctuation) into electricity, which shows prospective in thermal imaging, physiological monitoring, modulating interfacial charge transfer of heterojunctions, and powering micro/nanoscale electronics. [9–13] Basically, the pyroelectric effect originates from non-centrosymmetric piezoelectrics that possess temperature-dependent spontaneous polarizations, [14] such as lithium niobate (LNB), lead zirconate titanate (PZT), lead magnesium niobate-lead titanate (PMN-PT), and polyvinylidene fluoride (PVDF). In the context of energy harvesting, the overall performance of pyroelectric nanogenerators is always influenced by the tradeoff of pyroelectric coefficient, dielectric constant, dielectric loss and specific heat capacity. [15] Previous studies have focused on both improvement of pyroelectric materials and development of new device structures. [15–19] It is thus necessary to develop a universal method to compare the ability of various pyroelectric nanogenerators with different materials and architectures. Until now, a variety of figure-of-merits relevant to thermal detection have been derived based on the peak current or voltage signals. [20–24] However, little effort has been dedicated to developing a performance figure-of-merit relevant to pyroelectric energy harvesting, which not only helps to select pyroelectric materials but also can precisely estimate potential value of generated electricity.

In the present work, we report experimental measurements of the energy harvested by applying temperature fluctuation on commercially available PVDF film and PZT ceramic. Starting from the charge-voltage diagram, physical equations are developed to reveal the output characteristics of pyroelectric nanogenerators. After identifying substantial parameters in the process of heat energy to electricity conversion, we propose a figure-of-merit for energy-harvesting applications based on the pyroelectric effect, providing strategies for optimization of

* Corresponding author.
** Corresponding authors at: CAS Center for Excellence in Nanoscience, Beijing Institute of Nanoenergy and Nanosystems, Chinese Academy of Sciences, Beijing 100083, PR China.
E-mail addresses: wangyh@ms.xjb.ac.cn (Y. Wang), zlwang@binn.cas.cn (Z.L. Wang), yayang@binn.cas.cn (Y. Yang).

https://doi.org/10.1016/j.nanoen.2018.11.020
Received 9 October 2018; Received in revised form 6 November 2018; Accepted 8 November 2018
Available online 10 November 2018

pyroelectric nanogenerators from both material and structural views. On one side, the pyroelectric material should possess high pyroelectric coefficient, low volume specific heat capacity and relatively low permittivity to develop large electricity from temperature fluctuation. On the other side, one can estimate potential value of generated electricity based on the maximum temperature variation once the pyroelectric material is specified.

2. Experimental section

2.1. Device fabrication

The bottom side and top side of the commercial PVDF film (10 mm × 10 mm × 0.011 mm, ZHIMK) and bulk PZT (70 mm × 70 mm × 1 mm, HENGSHENG) were deposited with silver (Ag) layers as electrodes. Then, they were fixed on the surface of two commercial Peltier coolers, respectively. A commercial Peltier cooler supported by a radiator was fixed on an acrylic substrate to provide the temperature change. Finally, two copper wires were adhered to both sides of the pyroelectric elements using Ag paste, which were connected to the measurement system.

2.2. Characterization and measurements

Crystallographic information of the PVDF and PZT samples were collected using powder X-ray diffraction (XRD, Philips X'Pert [3] diffractometer, copper Kα radiation with λ = 1.54 Å). A scanning rate of 5°·min^{-1} was applied to record the patterns in the range 10 ~ 60° (2θ). To measure the performance of the pyroelectric nanogenerators, the device was placed on a commercial Peltier cooler to establish temperature change, and the temperature profiles were recorded by an IR thermographic camera (Optris PI400). The *I-t*, *V-t*, *Q-t* measurements were performed with a low-noise SourceMeter (Keithely 2611B).

3. Results and discussion

3.1. Pyroelectric characteristic and Q-V diagram

Fig. 1 illustrates the pyroelectric profile and working mechanism of a typical PVDF film material. The polarized PVDF film with both surfaces deposited with silver (Ag) as electrodes has a size of 10 × 10 × 0.1 mm. When the film is heated from 303 to 324 K, peak pyroelectric voltage of approximately − 28 V is produced at maximum heating rate of dT/dt = 1.8 K/s, as displayed in Fig. 1a. Ideally, square wave voltage/current profile will be produced from the pyroelectric material when the temperature changes uniformly with constant heating or cooling rate. By using the pyroelectric coefficient ($p = -2.7$ nC/cm^2·K) and active area (A = 1 cm^2) of the PVDF film, constant pyroelectric voltage was ideally calculated to be − 9.6 V from $V = IR = pAR(dT/dt)$ when the temperature increases from 303 to 324 K with constant heating rate of dT/dt = 0.35 K/s under load resistance of 10 GΩ. Recently, a performance figure-of-merit is well derived for the triboelectric nanogenerators from the charge-voltage (*Q-V*) cycles, [25] representing a standard for developing triboelectric nanogenerators towards practical applications. Fig. 1b depicts the charge generation process and corresponding *Q-V* diagram of a pyroelectric nanogenerator based on PVDF film. Initially, the oscillation of electric dipoles in PVDF reaches an equilibrium state at low temperature T_0 (dT/dt = 0), and no electron flow can be observed. As the temperature increases to T (dT/dt > 0), the electric dipoles oscillate within a larger degree of their respective alignment axes, leading to weaker spontaneous polarization. This causes an electrical imbalance, which drives the electrons to flow from the top to the bottom electrode in external electrical circuit. When the temperature reaches the maximum value of $T_0 + \Delta T$ (dT/dt = 0), the oscillation of electric dipoles reaches another equilibrium state at high temperature $T_0 + \Delta T$. At the moment, no electron flow occurs due to electrical balance. Afterwards, if the temperature of PVDF is decreased from $T_0 + \Delta T$ to T (dT/dt < 0), the spontaneous polarization

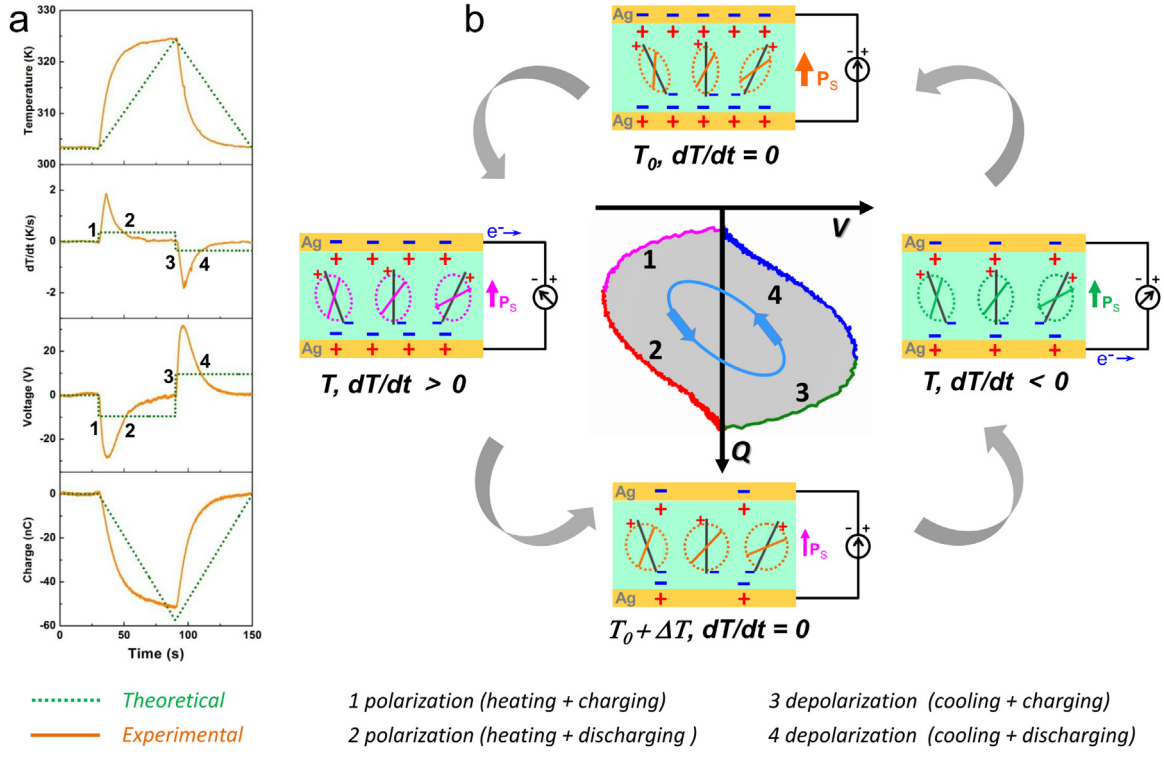

Fig. 1. Pyroelectric profile and mechanism of typical PVDF film material. (**a**) The ideal and real data of the temperature and pyroelectric profiles (temperature, rate of temperature change, voltage and charge) of a typical PVDF film material upon a whole heating process. (**b**) The charge generation process and representative charge-voltage (*Q-V*) diagram of a pyroelectric nanogenerator based on PVDF film.

within PVDF would be promoted, owing to stronger oscillation of electric dipoles. Thus, reverse electron flow from the bottom to the top electrode is observed under the driven of reverse pyroelectric potential. Until the temperature of PVDF is decreased to T_0, the electric dipoles regain their orientation and a full cycle of charge generation process finishes. The corresponding *Q-V* diagram is represented by the 1–2–3–4 loop in Fig. 1b. Unlike the Olsen cycle which consists of two isothermal and two isoelectric processes, [26,27] the real *Q-V* diagram of the PVDF film begins by charging the pyroelectric nanogenerator through heating the device from T_0 to T accompanied with increasing voltage (process 1). Then, the pyroelectric nanogenerator is further charged by heating the device from T to $T_0 + \Delta T$ accompanied with reducing voltage (process 2). Subsequently, the pyroelectric nanogenerator is discharged by decreasing the temperature from $T_0 + \Delta T$ to T with the increase of output voltage (process 3) and further decreasing the temperature from T to T_0 with the decrease of output voltage (process 4).

The governing equations of a pyroelectric nanogenerator can be developed on the basis of the *Q-V* relationship. The shaded area of the closed loop in the *Q-V* diagram in Fig. 1b corresponds to the output energy per cycle (E_{cycle}), which is given in Eq. (1):

$$E_{cycle} = \oint V dQ \tag{1}$$

3.2. Measured output energy of pyroelectric nanogenerator

Lead zirconate titanate ($Pb(Zr_xTi_{1-x})O_3$: PZT) and polyvinylidene fluoride (PVDF) have received considerable attention for their excellent pyroelectric properties. In this paper, both PVDF in film form and PZT in ceramic form are considered to quantify the performance of pyroelectric nanogenerators. The basic parameters of the PVDF and PZT are given in Table S1. Fig. 2a shows a 3-atom primitive cell of PVDF and a cubic unit cell of PZT. The PVDF is a semi-crystalline polymer with $-CF_2-CH_2-$ chain conformation. [28] The PZT has an ABO_3 type perovskite structure, [29] where Pb^{2+} ions occupy the A positions (corners of the cube), Zr^{4+} or Ti^{4+} ions occupy the B positions (body center), and O^{2-} ions occupy the face centers. Fig. 2b shows the X-ray diffraction (XRD) patterns of the PVDF film and bulk PZT. The XRD pattern of PVDF reveals semi-crystalline nature of the polymer. The two well-defined peaks at around $2\theta = 20.6$ is the characteristic peak of β-phase PVDF. [30–32] The β-phase PVDF possesses an all-trans (TTTT) zigzag chain conformation, where molecular dipoles associated with positive hydrogen and negative fluoride atoms are entirely aligned in the direction perpendicular to carbon backbone, resulting in the largest spontaneous polarization and the most superior pyroelectric properties. [33] For the bulk PZT, the XRD pattern depicts split peaks of (001)/(100), (101)/(110), (002)/(200) planes, and primarily crystallized in the tetragonal perovskite phase. [34] Fig. 2c displays the temperature oscillations applied to the pyroelectric materials. For PVDF film, the temperature is varied from 300 to 323 K with peak heating rate of $dT/dt = 7.6$ K/s. For bulk PZT, the temperature is varied from 300 to 308 K with peak heating rate of $dT/dt = 1.3$ K/s. As shown in Fig. 2d, negative current signals are observed upon increasing the temperature. A maximum output current of -4.5 nA was obtained at $dT/dt = 7.6$ K/s. From the *V-Q* plot (Fig. 2e and Fig. S1), we notice that the operation of the pyroelectric nanogenerator is steady during the measured periods, while a drift of the *V-Q* cycle happens, owing to the asymmetrical heat transmission between the heating process from T_0 to $T_0 + \Delta T$ and the cooling process $T_0 + \Delta T$ to T_0. The clockwise *V-Q* cycle indicates an energy given to the outside. As depicted in Fig. 2d, by integration of the output current towards time, the generated charges during the heating process and the cooling process was calculated to be 69 nC and 58 nC, respectively. For the bulk PZT, a maximum output current of 97 nA was obtained at $dT/dt = 1.3$ K/s (Fig. 2f), and a similar *Q-V* behavior was demonstrated (Fig. 2g). To be noted, the recovery time needed for the bulk PZT (> 550 s) is apparently longer than that for the PVDF film (> 50 s), mainly ascribed to the volume difference of the pyroelectric materials. Thus, different frequencies of temperature oscillations were applied to the bulk PZT and PVDF film to ensure complete recovery of material temperature.

To obtain optimal output power, we also measured the output currents and *Q-V* cycles for the pyroelectric nanogenerator based on PVDF and PZT under various external load resistances. As shown in Fig. 3a,b, the peak values of output currents decrease along with the increase of external load resistance. From the areas of these *Q-V* cycles, it can be seen that the output energy can be optimized by applying a matched load resistance (Fig. 3c,d). Besides, the total cycling charge Q_c (the difference between the maximum and minimum transferred charges in the *Q-V* cycle) decreases with increasing the external load resistance. In the short-circuit case, the transferred charge reaches the maximum value (Q_{sc}). Fig. 3e,f depicts the resistance-dependent instantaneous power calculated from the peak current ($I^2 R$) as well as the output energy per cycle obtained from absolute integration of the *Q-V* cycle. It is interesting to note that the changing trend of instantaneous power is coincident with that of the output energy per cycle. Under a load resistance of 50 GΩ, a maximized instantaneous power of 0.33 μW and output energy of 2.53 μJ per cycle are achieved for the pyroelectric nanogenerator based on PVDF film (10 × 10 mm). For the pyroelectric nanogenerator based on bulk PZT (49 × 49 mm), a maximized instantaneous power of 8.89 μW and output energy of 2.59 mJ per cycle are achieved under a load resistance of 1 GΩ.

3.3. Derived figure-of-merit for pyroelectric nanogenerator

For a pyroelectric nanogenerator, the electrical output signal depends on the period of temperature fluctuation, and the equivalent circuit can be modelled as a current source in parallel with the internal resistance R_P and the capacitance C_P (Fig. 4a). If the pyroelectric material is exposed to incident thermal radiation W (J/s), the thermal energy is converted into a temperature increase. To simplify, radiation is neglected in the process. Thus, given a certain cycle period τ (the radiation time is $\tau/2$), the maximum temperature increase can be calculated using Eq. (2):

$$\Delta T = \frac{W \cdot \tau}{2 \cdot c_E \cdot h \cdot A} \tag{2}$$

where c_E is the volume specific heat capacity, h is the thickness, and A is the surface area of the pyroelectric material. As a consequence, the average output power $\overline{P}$ can be mathematically expressed by Eq. (3):

$$\overline{P} = \frac{E_{cycle}}{\tau} = \frac{E_{cycle} \cdot W}{2 \cdot c_E \cdot h \cdot A \cdot \Delta T} \tag{3}$$

Regardless of the load resistance, the E_{cycle} is proportional to the product of the transferred charge and the output voltage. Assuming that the pyroelectric coefficient (p) is constant in the whole working temperature range, the transferred charge can be developed by integrating the output current with respect to time, as described in Eq. (4):

$$Q = \int_0^{\tau/2} I dt = \int_0^{\tau/2} pA \frac{dT}{dt} dt = \int_0^{\Delta T} pA dT = pA\Delta T \tag{4}$$

From Fig. 4a, we notice that the pyroelectric nanogenerator is equal to a parallel plate capacitor. In addition, the pyroelectric materials are typically dielectric in nature. So, the output voltage (V) across the electrodes can be expressed by Eq. (5):

$$V = \frac{Q}{C} = \frac{p}{\varepsilon_{33}} \cdot h \cdot \Delta T \tag{5}$$

where C is the capacitance of the equivalent circuit and ε_{33} is the permittivity of the pyroelectric material.

As indicated in Eqs. (4) and (5), the transferred charge is related to the effective surface area while the voltage is related to the material thickness. We notice that in Eq. (1), the E_{cycle} is proportional to the Q

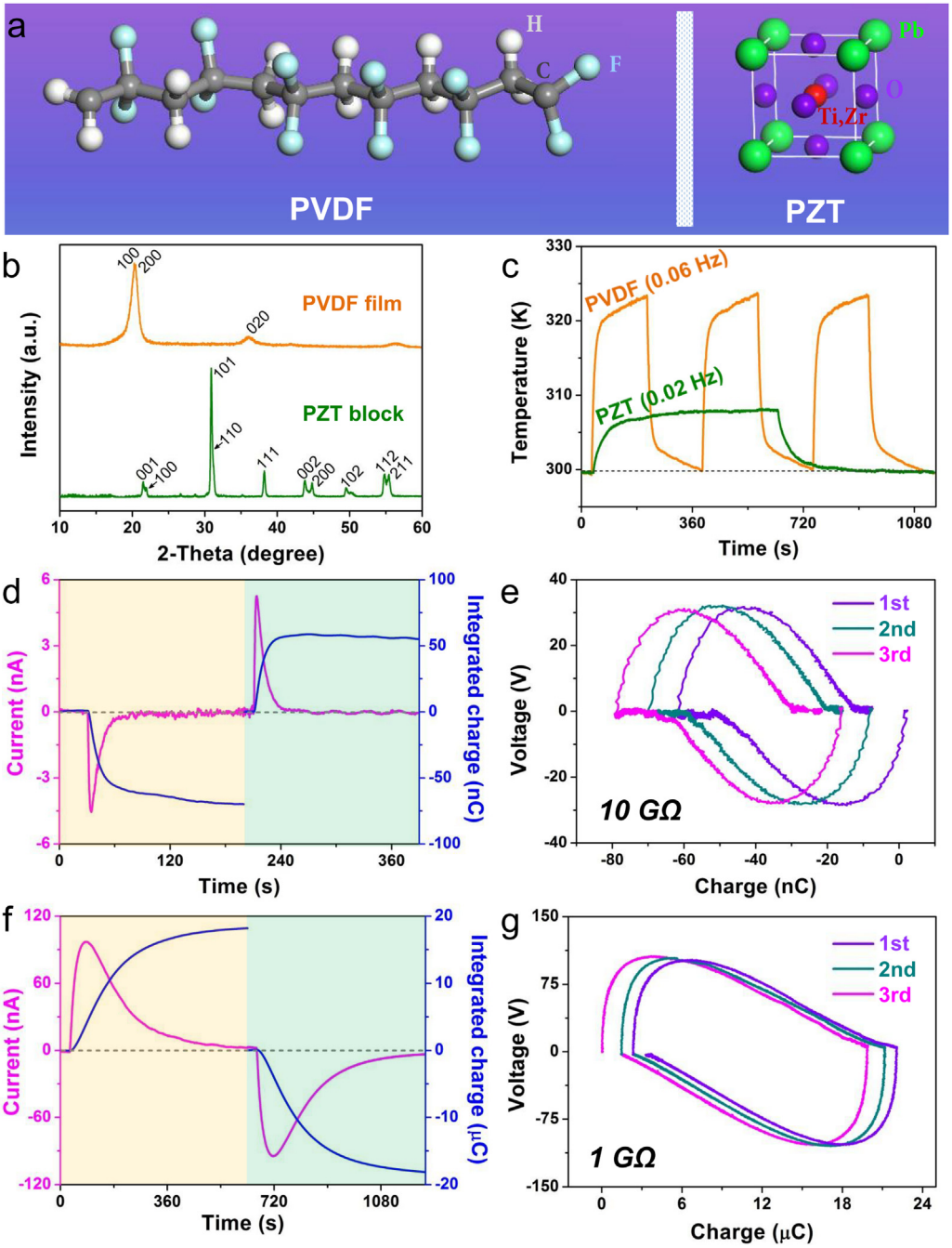

Fig. 2. Crystal structure and pyroelectric results of PVDF and PZT device. (a) A 3-atom primitive cell of PVDF and a cubic unit cell of PZT. (b) XRD patterns of the PVDF film and bulk PZT material. (c) The temperature oscillations applied to the PVDF film and bulk PZT material. (d,e) The pyroelectric current and corresponding integrated charges (d), and *Q-V* cycles (e) of PVDF film with load resistance of $R = 10\,\mathrm{G\Omega}$. (f,g) The pyroelectric current and corresponding integrated charges (f), and *Q-V* cycles (g) of bulk PZT with load resistance of $R = 1\,\mathrm{G\Omega}$.

and V. Substituting Eqs. (4) and (5) into Eq. (1), then into Eq. (3), we can reach Eq. (6) after rearranging.

$$\overline{P} \propto \frac{p^2 \cdot \Delta T \cdot W}{c_E \cdot \varepsilon_{33}} \tag{6}$$

Then, we can define a performance figure-of-merit (F_E'') of pyroelectric nanogenerator, as described in Eq. (7):

$$F_E'' = \frac{p^2 \Delta T}{c_E \varepsilon_{33}} \tag{7}$$

in which the c_E and ε_{33} are related to the material properties, while the ΔT is related to the input energy and the Curie temperature of the pyroelectric material. The F_E'' can be considered as a universal energy-harvesting standard to evaluate varieties of pyroelectric nanogenerators. As inferred from Eq. (7), the pyroelectric material should possess high pyroelectric coefficient, low volume specific heat capacity and low permittivity to develop large electricity from temperature fluctuation. Moreover, one can estimate potential value of generated electricity based on the maximum temperature variation (ΔT) once the pyroelectric material is specific.

In the context of thermal energy harvesting applications, three types of pyroelectric figure-of-merits have been derived previously. [35–37] Fig. 4b shows a comparison of various energy-harvesting figure-of-merits (k^2, F_E, F_E', F_E'') for selected PVDF and PZT materials. The k^2 is an

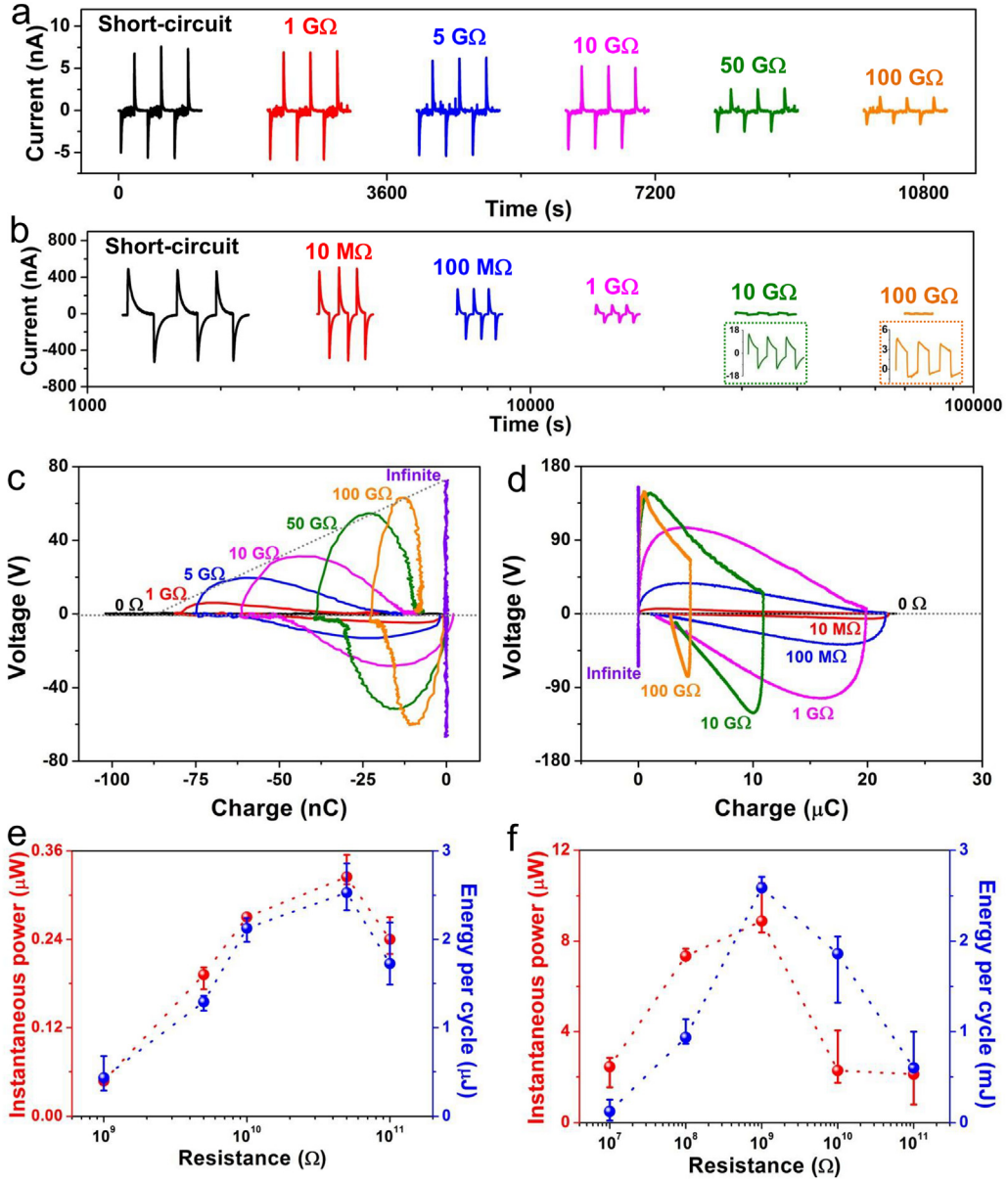

Fig. 3. Resistance-dependent energy conversion of pyroelectric PVDF and PZT. (a,b) The output currents of the (a) PVDF device and (b) PZT device under various load resistances. (c,d) The *Q-V* cycles of the (c) PVDF device and (d) PZT device under various load resistances. (e,f) The output powers of the (e) PVDF device and (f) PZT device under various load resistances.

electro-thermal coupling factor indicating how effectively a pyroelectric nanogenerator converts temperature fluctuation into electricity, while F_E, F_E' and F_E'' represents how much electricity a pyroelectric nanogenerator can harvest from the temperature fluctuation. As depicted in Fig. 4b, all the above figure-of-merits for bulk PZT is slightly larger than that for PVDF film, indicating superior pyroelectric performance of bulk PZT. The value of F_E'' is obviously large as compared to the value of modified F_E', owing to the high volume specific heat capacity and strong dependency on ΔT. Thereafter, the F_E'' is adopted to estimate the potential performance of conventional pyroelectric materials (Fig. 4c). The related parameters of pyroelectric materials were displayed in Table S1. The $LiTaO_3$ crystal, PMN-0.25PT ceramic and PZT ceramic remain high performance pyroelectric materials, while the CdS crystal, ZnO crystal and $BaTiO_3$ ceramic represent pyroelectric materials of low performance. We further experimentally confirm the practicability of F_E'' as a universal standard for pyroelectric nanogenerator. The *Q-V* cycles of the PVDF film and bulk PZT devices were rigorously measured under various temperature differences, as shown in Fig. 4d,e. For both the PVDF film and bulk PZT device, the electrical energy produced per unit volume of material per cycle exhibits a linear dependence on the temperature difference (Fig. 4f,g). It is of particular interest that the obtained linearity for the bulk PZT (0.0715 mJ cm^{-3}/K) is about 2.76 times larger than that for the PVDF film (0.0259 mJ cm^{-3}/K), which is consistent with the ratio (2.89 times) calculated from $p^2/(c_E\,\varepsilon_{33})$ using the parameters in Table S1. This result confirms that the F_E'' derived in this work is suitable for estimating the generated electricity of a pyroelectric nanogenerator.

4. Conclusion

In conclusion, this paper reports on direct heat energy to electricity conversion by performing charge-voltage cycles on commercial PVDF and PZT materials. When the PVDF in film form (10 × 10 mm) is heated from 300 to 323 K, a maximized instantaneous power of 0.33 μW and output energy of 2.53 μJ per cycle is achieved under a load resistance of 50 GΩ. Similarly, a maximized instantaneous power of 8.89

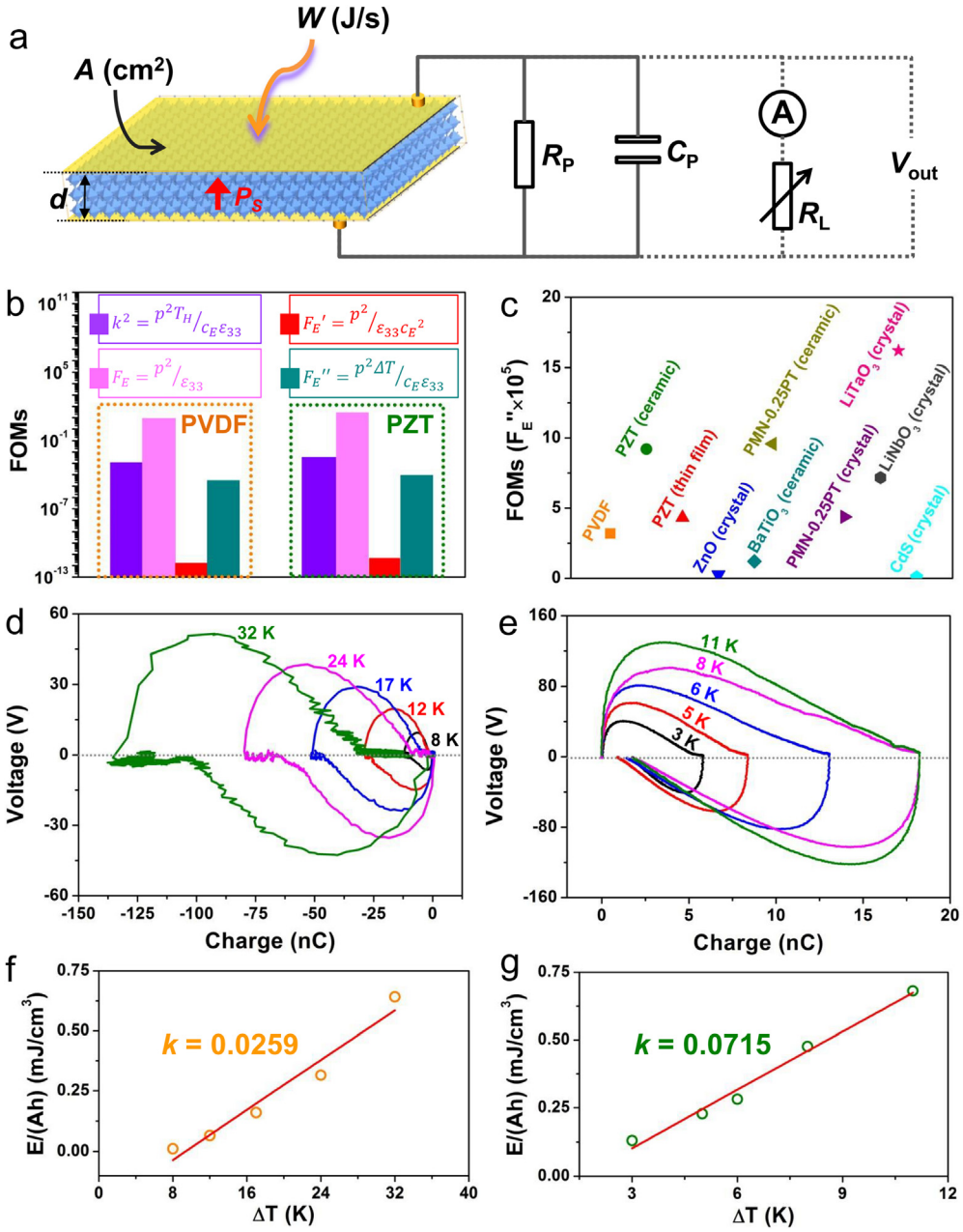

Fig. 4. Schematic and figure-of-merits of pyroelectric nanogenerator. (**a**) Electrical circuit of a pyroelectric nanogenerator which is modelled as a current source in parallel with the internal resistance R_P and the capacitance C_P. (**b**) Comparison of various figure-of-merits (k^2, F_E, F_E', F_E'') for the PVDF and PZT materials. T_{hot} = 298 K for k^2 (%), and ΔT = 8 K for F_E''. The unit of F_E and F_E' is $J{\cdot}m^{-3}{\cdot}K^{-2}$ and $m^3{\cdot}J^{-1}$, respectively, while the k^2 and F_E'' are dimensionless. (**c**) Examples of the figure-of-merit (F_E'') for a variety of pyroelectric materials. (**d,e**) The *Q-V* cycles of (d) the PVDF device and (e) the PZT device under various temperature differences. (**f,g**) ΔT-dependent output energy per unit volume for (f) the PVDF device and (g) the PZT device.

μW and output energy of 2.59 mJ per cycle is achieved for the PZT in ceramic form (49 × 49 mm) under a load resistance of 1 GΩ when the temperature is varied from 300 to 308 K. Starting from the charge-voltage cycle, physical equations are developed to reveal the total amount of harvested energy. Consequently, a figure-of-merit for energy-harvesting applications based on the pyroelectric effect was proposed to provide strategies for optimization of pyroelectric nanogenerators. The practicability of the newly derived figure-of-merit as a universal standard for pyroelectric nanogenerator was further experimentally confirmed. We believe that it could be useful for selecting proper pyroelectric material as well as estimating potential value of generated electricity based on maximum temperature fluctuation.

Acknowledgments

This work was supported by the National Key R&D Program of China (Grant No. 2016YFA0202701), the National Natural Science Foundation of China (Grant Nos. 61604012, 51472055, 61404034), External Cooperation Program of BIC, Chinese Academy of Sciences (Grant No. 121411KYS820150028), the 2015 Annual Beijing Talents Fund (Grant No. 2015000021223ZK32), Qingdao National Laboratory for Marine Science and Technology (No. 2017ASKJ01), and the Shenzhen Peacock Plan (Grant No. KQTD2015071616442225).

Appendix A. Supplementary material

Supplementary data associated with this article can be found in the online version at doi:10.1016/j.nanoen.2018.11.020.

References

[1] Y. Cheng, X. Lu, K.H. Chan, R. Wang, Z. Cao, J. Sun, G.W. Ho, Nano Energy 41 (2017) 511–518.
[2] Y. Zhang, M. Xie, V. Adamaki, H. Khanbareh, C.R. Bowen, Chem. Soc. Rev. 46 (2017) 7757–7786.
[3] H. Wu, Y. Huang, F. Xu, Y. Duan, Z. Yin, Adv. Mater. 28 (2016) 9881–9919.
[4] A.P. Straub, N.Y. Yip, S. Lin, J. Lee, M. Elimelech, Nat. Energy 1 (2016) 16090.
[5] X.Q. Wang, C.F. Tan, K.H. Chan, K. Xu, M. Hong, S.W. Kim, G.W. Ho, ACS Nano 11

(2017) 10568–10574.
[6] M. Vaish, M. Sharma, R. Vaish, V.S. Chauhan, Energy Technol. 3 (2015) 768–773.
[7] M.-K. Kim, M.-S. Kim, S. Lee, C. Kim, Y.-J. Kim, Smart Mater. Struct. 23 (2014) 105002.
[8] Y. Yang, K.C. Pradel, Q. Jing, J.M. Wu, F. Zhang, Y. Zhou, Y. Zhang, Z.L. Wang, ACS Nano 6 (2012) 6984–6989.
[9] H. Fang, C. Xu, J. Ding, Q. Li, J.L. Sun, J.Y. Dai, T.L. Ren, Q. Yan, ACS Appl. Mater. Interfaces 8 (2016) 32934–32939.
[10] Q. Leng, L. Chen, H. Guo, J. Liu, G. Liu, C. Hu, Y. Xi, J. Mater. Chem. A 2 (2014) 11940–11947.
[11] C.R. Bowen, J. Taylor, E. LeBoulbar, D. Zabek, A. Chauhan, R. Vaish, Energy Environ. Sci. 7 (2014) 3836–3856.
[12] K. Zhang, Z.L. Wang, Y. Yang, ACS Nano 10 (2016) 10331–10338.
[13] X. Wang, Y. Dai, R. Liu, X. He, S. Li, Z.L. Wang, ACS Nano 11 (2017) 8339–8345.
[14] S.B. Lang, Phys. Today 58 (2005) 31–36.
[15] K.S. Srikanth, V.P. Singh, R. Vaish, J. Eur. Ceram. Soc. 37 (2017) 3943–3950.
[16] M. Xie, D. Zabek, C. Bowen, M. Abdelmageed, M. Arafa, Smart Mater. Struct. 25 (2016) 125023.
[17] G. Vats, A. Kumar, N. Ortega, C.R. Bowen, R.S. Katiyar, Energy Environ. Sci. 9 (2016) 1335–1345.
[18] F. Gao, W. Li, X. Wang, X. Fang, M. Ma, Nano Energy 22 (2016) 19–26.
[19] D. Zabek, J. Taylor, E.L. Boulbar, C.R. Bowen, Adv. Energy Mater. 5 (2015) 1401891.
[20] C.P. Shaw, R.W. Whatmore, J.R. Alcock, J. Am. Ceram. Soc. 90 (2007) 137–142.
[21] R.W. Whatmore, J. Electroceram. 13 (2004) 139–147.
[22] T.G. Sweeney, R.W. Whatmore, Ferroelectrics 187 (1996) 57–73.
[23] R.W. Whatmore, Q. Zhang, C.P. Shaw, R.A. Dorey, J.R. Alcock, Phys. Scr. T129 (2007) 6–11.
[24] Z. Huang, P.P. Donohue, Q. Zhang, D.J. Williams, C.J. Anthony, R.W. Whatmore, M.A. Todd, J. Phys. D: Appl. Phys. 36 (2003) 270–279.
[25] Y. Zi, S. Niu, J. Wang, Z. Wen, W. Tang, Z.L. Wang, Nat. Commun. 6 (2015) 8376.
[26] R. Kandilian, A. Navid, L. Pilon, Smart Mater. Struct. 20 (2011) 055020.
[27] R.B. Olsen, J. Energy 6 (1982) 91–95.
[28] S. Satapathy, S. Pawar, P.K. Gupta, K.B.R. Varma, Bull. Mater. Sci. 34 (2011) 727–733.
[29] N. Izyumskaya, Y.I. Alivov, S.J. Cho, H. Morkoç, H. Lee, Y.S. Kang, Crit. Rev. Solid State 32 (2007) 111–202.
[30] B. Dutta, E. Kar, N. Bose, S. Mukherjee, RSC Adv. 5 (2015) 105422–105434.
[31] R. Gregorio, J. Appl. Polym. Sci. 100 (2006) 3272–3279.
[32] X. Guan, Y. Zhang, H. Li, J. Ou, Sens. Actuators, A 194 (2013) 228–231.
[33] G. Zhu, Z. Zeng, L. Zhang, X. Yan, Comp. Mater. Sci. 44 (2008) 224–229.
[34] Z.J. Wang, Y. Aoki, L.J. Yan, H. Kokawa, R. Maeda, J. Cryst. Growth 267 (2004) 92–99.
[35] G. Sebald, E. Lefeuvre, D. Guyomar, IEEE Trans. Ultrason. Ferroelectr. Freq. Control 55 (2008) 538–551.
[36] G. Sebald, L. Seveyrat, D. Guyomar, L. Lebrun, B. Guiffard, S. Pruvost, J. Appl. Phys. 100 (2006) 124112.
[37] C.R. Bowen, J. Taylor, E.L. Boulbar, D. Zabek, V.Y. Topolov, Mater. Lett. 138 (2015) 243–246.

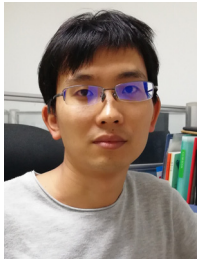

Dr. Kewei Zhang received his Ph.D in Chemical Engineering and Technology from Beijing University of Chemical Technology, China. He is currently an assistant professor at Beijing Institute of Nanoenergy and Nanosystems, Chinese Academy of Sciences (CAS). His research interests focus on nanogenerators and self-powered systems.

Prof. Yuanhao Wang received his BSc from the Tsinghua University and Ph.D in The Hong Kong Polytechnic University. He is currently the professor at the Xinjiang Technical Institute of Physics & Chemistry, CAS. His research interests focus on nanomaterials for green buildings and nanogenerators.

Prof. Zhong Lin (ZL) Wang received his Ph.D from Arizona State University in physics. He now is the Hightower Chair in Materials Science and Engineering, Regents' Professor, Engineering Distinguished Professor and Director, Center for Nanostructure Characterization, at Georgia Tech. Dr. Wang has made original and innovative contributions to the synthesis, discovery, characterization and understanding fundamental physical properties of oxide nanobelts and nanowires, as well as applications of nanowires in energy sciences, electronics, optoelectronics and biological science. His discovery and breakthroughs in developing nanogenerators established the principle and technological roadmap for harvesting mechanical energy from the environment and biological systems for powering a personal electronics. His research on self-powered nanosystems has inspiredthe worldwide effort in academia and industry for studying energy of or micro- nano-systems, which is now a distinct disciplinary in energy research and future sensor networks. He coined and pioneered the field of piezotronics and piezo-phototronics by introducing piezoelectric potential gated charge transport process in fabricating new electronic and optoelectronic devices. Details can be found at: http://www.nanoscience.gatech.edu.

Prof. Ya Yang received his Ph.D in Materials Science and Engineering from University of Science and Technology Beijing, China. He is currently a professor at Beijing Institute of Nanoenergy and Nanosystems, CAS. His main research interests focus on the field of pyroelectric, piezoelectric, triboelectric, and thermoelectric nanogenerators for energy conversion, storage and some novel applications.